

Long GRBs as a Tool to Investigate Star Formation in Dark Matter Halos

Jun-Jie Wei^a, Jing-Meng Hao^{b,c}, Xue-Feng Wu^{a,d,*}, Ye-Fei Yuan^e

^a*Purple Mountain Observatory, Chinese Academy of Sciences, Nanjing 210008, China*

^b*Center for Astrophysics, Guangzhou University, Guangzhou 510006, China*

^c*Astronomy Science and Technology Research Laboratory of Department of Education of Guangdong Province, Guangzhou 510006, China*

^d*Joint Center for Particle, Nuclear Physics and Cosmology, Nanjing University-Purple Mountain Observatory, Nanjing 210008, China*

^e*Key Laboratory for Research in Galaxies and Cosmology CAS, Department of Astronomy, University of Science and Technology of China, Hefei, Anhui 230026, China*

Abstract

First stars can only form in structures that are suitably dense, which can be parametrized by the minimum dark matter halo mass M_{\min} . M_{\min} must play an important role in star formation. The connection of long gamma-ray bursts (LGRBs) with the collapse of massive stars has provided a good opportunity for probing star formation in dark matter halos. We place some constraints on M_{\min} using the latest *Swift* LGRB data. We conservatively consider that LGRB rate is proportional to the cosmic star formation rate (CSFR) and an additional evolution parametrized as $(1+z)^\alpha$, where the CSFR model as a function of M_{\min} . Using the χ^2 statistic, the contour constraints on the M_{\min} - α plane show that at the 1σ confidence level, we have $M_{\min} < 10^{10.5} M_\odot$ from 118 LGRBs with redshift $z < 4$ and luminosity $L_{\text{iso}} > 1.8 \times 10^{51} \text{ erg s}^{-1}$. We also find that adding 12 high- z ($4 < z < 5$) LGRBs (consisting of 104 LGRBs with $z < 5$ and $L_{\text{iso}} > 3.1 \times 10^{51} \text{ erg s}^{-1}$) could result in much tighter constraints on M_{\min} , for which, $10^{7.7} M_\odot < M_{\min} < 10^{11.6} M_\odot$ (1σ). Through Monte Carlo simulations, we estimate that future five years of Sino-French spacebased multiband astronomical variable objects monitor (*SVOM*) observations would tighten these constraints to

*Corresponding author.

Email addresses: xfwu@pmo.ac.cn (Xue-Feng Wu), yfyuan@ustc.edu.cn (Ye-Fei Yuan)

$10^{9.7}M_{\odot} < M_{\min} < 10^{11.3}M_{\odot}$. The strong constraints on M_{\min} indicate that LGRBs are a new promising tool for investigating star formation in dark matter halos.

Keywords: Gamma-ray burst: general, galaxy: evolution, stars: formation.

1. Introduction

Gamma-ray bursts (GRBs) are the most luminous explosive events in the cosmos, which can be detected even out to the edge of the Universe. To date, the highest redshift of GRBs is ~ 9.4 (GRB 090429B; Cucchiara et al., 2011). So GRBs are considered as a powerful tool to probe the properties of the high- z Universe, including high- z star formation history (e.g., Chary, Berger, & Cowie, 2007; Yüksel et al., 2008; Kistler et al., 2009; Trenti et al., 2012; Wei et al., 2014), metal enrichment history (Wang et al., 2012), and the dark matter particle mass (de Souza et al., 2013). Theoretically, it is widely accepted that long bursts (LGRBs) with durations $T_{90} > 2$ s (where T_{90} is the interval observed to contain 90% of the prompt emission; Kouveliotou et al., 1993) are powered by the core collapse of massive stars (e.g., Woosley, 1993; Paczyński, 1998; Woosley & Bloom, 2006), which have been strongly supported by several confirmed associations between LGRBs and Type Ic supernovae (Stanek et al., 2003; Hjorth et al., 2003; Chornock et al., 2010). The collapsar model suggests that the cosmic GRB rate should in principle trace the cosmic star formation rate (CSFR; Totani, 1997; Wijers et al., 1998; Blain & Natarajan, 2000; Lamb & Reichart, 2000; Porciani & Madau, 2001; Piran, 2004; Zhang & Mészáros, 2004; Zhang, 2007).

Thanks to the great contribution of the *Swift* satellite (Gehrels et al., 2004), the number of GRBs with measured redshifts has increased rapidly over the last decade. Surprisingly, the *Swift* data seems to indicate that the rate of LGRBs does not strictly trace the CSFR, but instead implying some kind of additional evolution (Daigne, Rossi, & Mochkovitch, 2006; Guetta & Piran, 2007; Le & Dermer, 2007; Salvaterra & Chincarini, 2007; Kistler et al., 2008, 2009; Li, 2008; Salvaterra et al., 2009, 2012; Campisi, Li, & Jakobsson, 2010; Qin et al., 2010; Wanderman & Piran, 2010; Cao et al., 2011; Virgili et al., 2011; Elliott et al., 2012; Lu et al., 2012; Robertson & Ellis, 2012; Wang, 2013; Wei et al., 2014). The observed discrepancy between the LGRB rate and the CSFR is used to be described by an enhanced evolution parametrized as $(1+z)^{\alpha}$ (e.g., Kistler et al., 2008). Many mechanisms have been proposed

to explain the enhancement, such as cosmic metallicity evolution (Langer & Norman, 2006; Li, 2008), an evolution in the stellar initial mass function (Xu & Wei, 2009; Wang & Dai, 2011), and an evolution in the GRB luminosity function (Virgili et al., 2011; Salvaterra et al., 2012; Tan, Cao, & Yu, 2013; Tan & Wang, 2015).

However, it should be emphasized that the prediction on the LGRB rate strongly relates to the star formation rate models. With different star formation history models, the results on the discrepancy between LGRB rate and CSFR could change in some degree (see Virgili et al., 2011; Hao & Yuan, 2013). There are many forms of CSFR available in the literature. Most previous studies (e.g., Kistler et al., 2008, 2009; Li, 2008; Salvaterra et al., 2009, 2012; Robertson & Ellis, 2012; Wei et al., 2014) adopted the widely accepted CSFR model of Hopkins & Beacom (2006), which provides a good piecewise-linear fit to the ultraviolet and far-infrared observations. But, it is obviously that the empirical fit will vary depending on both the functional form and the observational data used. Hao & Yuan (2013) confirmed that LGRBs were still biased tracers of the CSFR model derived from the empirical fit of Hopkins & Beacom (2006). While, using the self-consistent CSFR model calculated from the hierarchical structure formation scenario, they found that large number of LGRBs occur in dark matter halos with mass down to $10^{8.5}M_{\odot}$ could give an alternative explanation for the CSFR–LGRB rate discrepancy.

The fact that stars can only form in structures that are suitably dense, which can be parametrized by the minimum mass M_{\min} of a dark matter halo of the collapsed structures where star formation occurs. Structures with masses smaller than M_{\min} are considered as part of the intergalactic medium and do not take part in the star formation process. Thus, the minimum halo mass M_{\min} must plays an important role in star formation. Some observational data have been used to constrain M_{\min} in several instance, including the following representative cases: Daigne et al. (2006) showed that with a minimum halo mass of $10^7 - 10^8 M_{\odot}$ and a moderate outflow efficiency, they were able to reproduce both the current baryon fraction and the early chemical enrichment of the intergalactic medium; Bouché et al. (2010) found that a minimum halo mass $M_{\min} \simeq 10^{11} M_{\odot}$ was required in their model to simultaneously account for the observed slopes of the star formation rate–mass and Tully–Fisher relations; Muñoz & Loeb (2011) found that the observed galaxy luminosity function was best fit with a minimum halo mass per galaxy of $10^{9.4^{+0.3}_{-0.9}} M_{\odot}$.

The collapsar model suggests that LGRBs constitute an ideal tool to investigate star formation in dark matter halos. The expected GRB redshift distributions can be calculated from the self-consistent CSFR model as a function of the minimum halo mass M_{\min} . Thus, M_{\min} can be constrained by directly comparing the observed and expected redshift distributions. In this paper, we extend the work of Hao & Yuan (2013) by presenting robust limits on M_{\min} using the latest *Swift* GRB data. Since the latest data have many redshift measurements, a reliable statistical analysis is now possible. This analysis not only provides a better understanding of the high- z CSFR using the LGRB data, but also indicates that LGRBs can be a new tool to constrain the minimum halo mass. The outline of this paper is as follows. In Section 2, we will briefly describe the star formation model we have adopted and demonstrate the impact of the minimum halo mass M_{\min} on the CSFR. In Section 3, we will present the method for calculating the theoretical GRB redshift distribution, and then in Section 4 show direct constraints on the numerical value of M_{\min} from the latest *Swift* GRB data. In Section 5, we will discuss possible future constraints using a mock sample. Finally, we will end with our conclusions in Section 6.

Throughout we use the cosmological parameters from the *Wilkinson Microwave Anisotropy Probe* (WMAP) nine-year data release (Hinshaw et al., 2013), namely $\Omega_{\text{m}} = 0.286$, $\Omega_{\Lambda} = 0.714$, $\Omega_{\text{b}} = 0.0463$, $\sigma_8 = 0.82$ and $h = 0.69$.

2. The cosmic star formation

In the framework of hierarchical structure formation, the self-consistent CSFR model can be obtained by solving the evolution equation of the total gas density that takes into account the baryon accretion rate, the ejection of gas by stars, and the stars formed through the transfer of baryons in the dark matter halos (see Pereira & Miranda, 2010). The baryon accretion rate stands for the process of structure formation, which governs the size of the reservoir of baryons available for star formation (Daigne et al., 2006). In this section, we will briefly summarize how to obtain the CSFR from the hierarchical model, which is developed by Pereira & Miranda (2010).

In the hierarchical formation scenario, the comoving abundance of collapsed dark matter halos can be determined based on the Press–Schechter (P–S) like formalism (Press & Schechter, 1974). We adopt the most popularly used halo mass function, named the Sheth–Tormen mass function

(Sheth & Tormen, 1999), which is similar to the form of the P–S mass function:

$$f_{\text{ST}}(\sigma) = A \sqrt{\frac{2a_1}{\pi}} \left[1 + \left(\frac{\sigma^2}{a_1 \delta_c^2} \right)^p \right] \frac{\delta_c}{\sigma} \exp \left(-\frac{a_1 \delta_c^2}{2\sigma^2} \right), \quad (1)$$

where the parameter $\delta_c = 1.686$ could be explained physically as the linearly extrapolated overdensity of a top-hat spherical density perturbation at the time of maximum compression. The choice of values $A = 0.3222$, $a_1 = 0.707$, and $p = 0.3$ gives the best fit to mass functions derived from numerical simulations over a broad range of redshifts and masses. The number density of dark matter halos with mass M , $n_{\text{ST}}(M, z)$, can be related to $f_{\text{ST}}(\sigma)$ by

$$\frac{dn_{\text{ST}}(M, z)}{dM} = \frac{\rho_m}{M} \frac{d \ln \sigma^{-1}}{dM} f_{\text{ST}}(\sigma), \quad (2)$$

where ρ_m is the mean mass density of the Universe. The variance of the linearly density field $\sigma(M, z)$ is given by

$$\sigma^2(M, z) = \frac{D^2(z)}{2\pi^2} \int_0^\infty k^2 P(k) W^2(k, M) dk, \quad (3)$$

where the primordial power spectrum $P(k)$ is smoothed with a real space top-hat filter function $W(k, M)$, $D(z)$ is the growth factor of linear perturbations normalized to $D = 1$ at the present epoch and the redshift dependence enters only through $D(z)$.

The baryon distribution is considered to be tracing the dark matter distribution without any bias, which means the baryons density is completely proportional to the density of dark matter. Note that first stars can form only in structures that are suitably dense, which can be parametrized by the minimum dark matter halo mass M_{min} . Thus, star formation will be suppressed when the halo mass below M_{min} . In fact, the suppression in star formation is time dependent, i.e., the minimum mass M_{min} should evolve with z as the cooling processes of the hot gas in structures depend on the chemical composition and ionizing state of the gas (see Daigne et al., 2006). However, the process of evolution is very complex. It is beyond the scope of this study to consider the detailed analysis on evolution, so we would like to keep M_{min} as a constant and set it as a free parameter in this model, as those authors did in their works (see, e.g., Daigne et al., 2006; Pereira & Miranda, 2010; Muñoz & Loeb, 2011). Therefore, the fraction of baryons inside collapsed

halos at redshift z is given by

$$f_b(z) = \frac{\int_{M_{\min}}^{\infty} n_{\text{ST}}(M, z) M \, dM}{\int_0^{\infty} n_{\text{ST}}(M, z) M \, dM} . \quad (4)$$

With the fraction, the baryons accretion rate $a_b(t)$ as a function of redshift, which accounts for the formation of structures, can be calculated by

$$a_b(t) = \Omega_b \rho_c \left(\frac{dt}{dz} \right)^{-1} \left| \frac{df_b(z)}{dz} \right| , \quad (5)$$

where $\rho_c = 3H_0^2/8\pi G$ is the critical density of the Universe.

For ease of calculation, we consider the star formation rate satisfying the Schmidt law (Schmidt, 1959, 1963), as Pereira & Miranda (2010) did in their treatment. The Schmidt law suggests that the star formation rate $\dot{\rho}_\star(t)$ is directly proportional to the local gas density $\rho_g(t)$, which can be simply expressed as

$$\frac{d^2 M_\star}{dV dt} = \dot{\rho}_\star(t) = k \rho_g(t) , \quad (6)$$

where k is a constant.

The mass ejected from stars, which is returned to the interstellar medium through winds and supernovae, is given by

$$\frac{d^2 M_{\text{ej}}}{dV dt} = \int_{m(t)}^{m_{\text{sup}}} (m - m_r) \Phi(m) \dot{\rho}_\star(t - \tau_m) \, dm , \quad (7)$$

where $m(t)$ corresponds to the stellar mass whose lifetime is equal to t . The mass of the remnant, m_r , depends on the progenitor mass (see Pereira & Miranda, 2010). The stellar initial mass function $\Phi(m)$ follows the Salpeter (1955) form, $\Phi(m) = A m^{-2.35}$, with the mass range $[m_{\text{inf}}, m_{\text{sup}}]$, where $m_{\text{inf}} = 0.1 \, M_\odot$ and $m_{\text{sup}} = 140 \, M_\odot$. τ_m is the lifetime of a star with mass m , which is calculated using the metallicity-independent fit of Scalo (1986) and Copi (1997).

Combining Equations (5), (6) and (7), the evolution of the total gas density (ρ_g) that determines the star formation history in the dark matter halos can be written down as

$$\dot{\rho}_g = - \frac{d^2 M_\star}{dV dt} + \frac{d^2 M_{\text{ej}}}{dV dt} + a_b(t) . \quad (8)$$

Finally, we can produce the function $\rho_g(t)$ at each time t (or redshift z) by solving Equation (8). Once obtained $\rho_g(t)$, we can calculate the CSFR $\dot{\rho}_*(t)$ according to Equation (6), i.e., $\dot{\rho}_* = k\rho_g$, where the constant $k = 1/\tau_s$ denotes the inverse of the timescale for star formation. Consistent with previous works (see, e.g., Pereira & Miranda, 2010; Hao & Yuan, 2013), we use $\tau_s = 2.0$ Gyr as the timescale of star formation and consider that the star formation starts at redshift $z_{\text{ini}} = 20$. The CSFR is normalized to $\dot{\rho}_* = 0.016 \text{ M}_\odot \text{ yr}^{-1} \text{ Mpc}^{-3}$ at $z = 0$ (Hopkins, 2004, 2007).

In Fig. 1, we show the CSFR obtained from the self-consistency models as a function of the minimum halo mass M_{min} (see Equation 4). The observational CSFR taken from Hopkins (2004, 2007) and Li (2008), which are based on the observations of other authors who are listed in these publications, are also shown for comparison. One can see from this plot that $\dot{\rho}_*(z)$ is very sensitive to the minimum mass M_{min} , especially at high- z . In addition, all of these models have good agreement with observational data at $z \leq 6$.

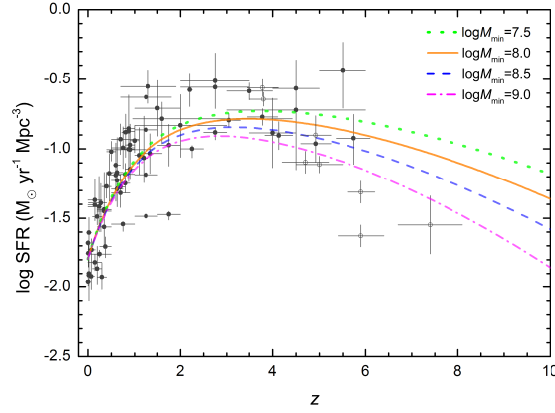


Figure 1: The CSFR $\dot{\rho}_*(z)$ derived from the self-consistency models compared to the observational data taken from Hopkins (2004, 2007) (dots) and Li (2008) (circles). The curves represent models with a minimum halo mass $M_{\text{min}} = 10^{7.5} \text{ M}_\odot$, $10^{8.0} \text{ M}_\odot$, $10^{8.5} \text{ M}_\odot$, and $10^{9.0} \text{ M}_\odot$, respectively.

3. The GRB technique

As discussed above, we assume that the relationship between the comoving GRB rate and the CSFR density $\dot{\rho}_*$ can be expressed as $\dot{n}_{\text{GRB}}(z) = \varepsilon(z)\dot{\rho}_*(z)$, where $\varepsilon(z)$ accounts for the formation efficiency of LGRBs. Note that the CSFR can be obtained from the self-consistency model with a free

parameter M_{\min} as described in Section 2. The expected redshift distribution of GRBs is given as

$$\frac{dN}{dz} = F(z) \frac{\varepsilon(z) \dot{\rho}_*(z)}{\langle f_{\text{beam}} \rangle} \frac{dV_{\text{com}}/dz}{1+z}, \quad (9)$$

where $F(z)$ represents the ability both to detect the GRB and to obtain the redshift, $\langle f_{\text{beam}} \rangle$ is the beaming factor, the factor $(1+z)^{-1}$ accounts for the cosmological time dilation, and dV_{com}/dz is the comoving volume element. As discussed in detail in Kistler et al. (2008), $F(z)$ can be treated as a constant (F_0) when we only consider the bright bursts with luminosities sufficient to be observed within an entire redshift range.

There is a general agreement about the fact that the LGRB rate does not strictly follow the CSFR but is actually enhanced by some unknown mechanisms at high- z . Several evolution scenarios have been considered to explain the observed enhancement, including the GRB rate density evolution (Kistler et al., 2008, 2009), cosmic metallicity evolution (Langer & Norman, 2006; Li, 2008), stellar initial mass function evolution (Xu & Wei, 2009; Wang & Dai, 2011), and luminosity function evolution (Virgili et al., 2011; Salvaterra et al., 2012; Tan, Cao, & Yu, 2013; Tan & Wang, 2015). In a word, there are much debate in the mechanisms responsible for the enhancement. For simplicity, we adopt the density evolution model and parametrize the evolution in the GRB rate as $\varepsilon(z) = \varepsilon_0(1+z)^\alpha$, where ε_0 is a constant that includes the fraction of stars that produce long GRBs. Here, we conservatively keep α as a free parameter. So there are two free parameters M_{\min} and α in our calculation.

The expected number of GRBs within a redshift range $z_1 \leq z \leq z_2$, for each combination $\mathbf{P} \equiv \{M_{\min}, \alpha\}$, can be described as

$$\begin{aligned} N(z_1, z_2; \mathbf{P}) &= \Delta t \frac{\Delta\Omega}{4\pi} \int_{z_1}^{z_2} F(z) \varepsilon(z) \frac{\dot{\rho}_*(z; M_{\min})}{\langle f_{\text{beam}} \rangle} \frac{dV_{\text{com}}/dz}{1+z} dz \\ &= \mathcal{A} \int_{z_1}^{z_2} (1+z)^\alpha \dot{\rho}_*(z; M_{\min}) \frac{dV_{\text{com}}/dz}{1+z} dz, \end{aligned} \quad (10)$$

where the constant $\mathcal{A} = \Delta t \Delta\Omega F_0 \varepsilon_0 / 4\pi \langle f_{\text{beam}} \rangle$ depends on the total observed time, Δt , and the angular sky coverage, $\Delta\Omega$. In order to remove the dependence on \mathcal{A} , we can simply construct the cumulative redshift distribution of GRBs over the redshift range $0 < z < z_{\text{max}}$, normalized to $N(0, z_{\text{max}})$, as

$$N(< z | z_{\text{max}}) = \frac{N(0, z)}{N(0, z_{\text{max}})}. \quad (11)$$

4. Constraints from *Swift* long GRBs

Our LGRB sample is taken from Wei et al. (2014), which is consisted of long GRBs detected by *Swift* up to 2013 July. Most of the data are collected from the samples presented in Butler et al. (2007); Butler, Bloom, & Poznanski (2010) and Sakamoto et al. (2011). Redshift measurements are strongly bi-ased towards optically bright afterglows, and are more easily made when the afterglow is not obscured by dust (see e.g. Greiner et al., 2011). The phenomenon of so-called dark GRBs with suppressed optical counterparts could influence whether the observed cumulative redshift distribution $N(< z)$ is representative of that for all long GRBs. Therefore, it is important to add the redshift of dark GRBs. Wei et al. (2014) also included dark GRBs from Perley et al. (2009), Greiner et al. (2011), Krühler et al. (2011), Hjorth et al. (2012), and Perley & Perley (2013).¹ With the information of redshift z , burst duration T_{90} , and isotropic-equivalent energy E_{iso} for each GRB taken from Wei et al. (2014), we calculate the isotropic-equivalent luminosities using $L_{\text{iso}} = E_{\text{iso}}/[T_{90}/(1+z)]$.

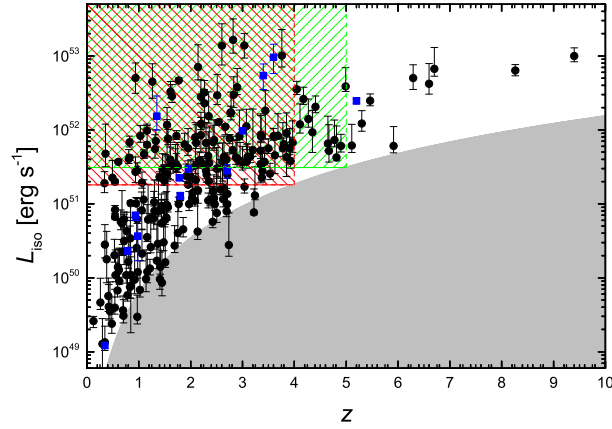


Figure 2: The luminosity-redshift distribution of 244 *Swift* GRBs from the catalog of Wei et al. (2014). The blue squares represent 13 dark bursts with firm redshift determinations. The gray shaded region approximates the *Swift* detection threshold. The red box corresponds to 118 GRBs with $z < 4$ and $L_{\text{iso}} > 1.8 \times 10^{51} \text{ erg s}^{-1}$, and the green box corresponds to 104 GRBs with $z < 5$ and $L_{\text{iso}} > 3.1 \times 10^{51} \text{ erg s}^{-1}$.

Our final sample includes 244 GRBs with firm redshift determinations, whose luminosity-redshift distribution is shown in Fig. 2. The shaded region

¹Several of the dark bursts with redshift upper limits are not included in this work.

represents the effective detection threshold of *Swift*. The luminosity threshold can be approximated using a bolometric energy flux limit $F_{\text{lim}} = 1.2 \times 10^{-8}$ erg cm $^{-2}$ s $^{-1}$ (Kistler et al., 2008), i.e., $L_{\text{lim}} = 4\pi D_L^2 F_{\text{lim}}$, where D_L is the luminosity distance. The sensitivity of *Swift*/Burst Alert Telescope (BAT) is very difficult to parametrize exactly (Band, 2006). In order to avoid the influence of *Swift* threshold, we will adopt a model-independent approach by selecting only GRBs with $L_{\text{iso}} > L_{\text{lim}}$ and $z < 4$, as Kistler et al. (2008) did in their treatment. The cut in luminosity is chosen to be equal to the threshold at the highest redshift of the sample, i.e., $L_{\text{lim}}(z = 4) \approx 1.8 \times 10^{51}$ erg s $^{-1}$. The cut in luminosity and redshift can reduce the selection effects by removing many low- z , low- L_{iso} bursts that could not have been observed at higher redshift. With these conditions, we have 118 GRBs in this sub-sample. These data are delimited by the red shaded region in Fig. 2.

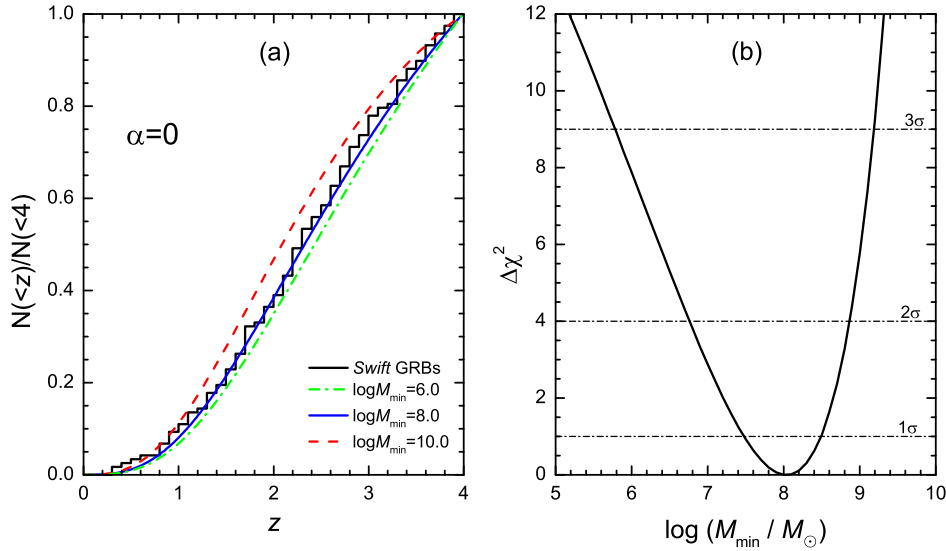


Figure 3: (a): cumulative redshift distribution of 118 *Swift* GRBs with $z < 4$ and $L_{\text{iso}} > 1.8 \times 10^{51}$ erg s $^{-1}$ (steps). The expected redshift distributions inferred from the self-consistent star formation rate model for $\alpha = 0$ as a function of the minimum halo mass M_{min} are also shown (from bottom to top): the green dot-dashed line corresponds to $M_{\text{min}} = 10^{6.0} M_{\odot}$, the blue solid line corresponds to $M_{\text{min}} = 10^{8.0} M_{\odot}$, and the red dashed line corresponds to $M_{\text{min}} = 10^{10.0} M_{\odot}$. (b): constraints on the minimum halo mass, M_{min} , for the $\alpha = 0$ model.

Fig. 3(a) shows the cumulative redshift distribution of these 118 GRBs (steps), as well as the expected redshift distributions inferred from the self-consistent CSFR model (curves). To evaluate the consistency between the

observed and the expected GRB redshift distributions, we make use of the one-sample Kolmogorov-Smirnov (K-S) test. In Fig. 3(a), we firstly consider the non-evolution case (i.e., the evolutionary index $\alpha = 0$), and compare the observed GRB cumulative redshift distribution with the expected distribution for different values of M_{\min} . We can find that the expectations from the models with a minimum halo mass $M_{\min} = 10^{6.0} M_{\odot}$ (green dot-dashed line) or $M_{\min} = 10^{10.0} M_{\odot}$ (red dashed line) are incompatible with the observations. The test statistics and probability for the relevant models are presented in Table 1. While, the model with $M_{\min} = 10^{8.0} M_{\odot}$ (blue solid line) can reproduce the observed data very well, with a maximum K-S probability of $P = 0.993$, which is consistent with that of Hao & Yuan (2013). This result implies that most of LGRBs occur in small dark matter halos down to $10^{8.0} M_{\odot}$ can provide an alternative explanation for the discrepancy between the LGRB rate and the CSFR, without considering the extra evolution effect (i.e., $\alpha = 0$).

In order to find the best-fit parameters together with their 1σ (or 2σ) confidence level, we also optimize the model fits by minimizing the χ^2 statistic

$$\chi^2 = \sum_i^n \frac{[N^{\text{th}}(< z_i | z_{\max}) - N^{\text{obs}}(< z_i | z_{\max})]^2}{\sigma_i^2}, \quad (12)$$

where n is the number of z bins, $N^{\text{th}}(< z_i | z_{\max})$ and $N^{\text{obs}}(< z_i | z_{\max})$ are the expected and the observed (normalized) cumulative numbers of LGRBs in bin i , respectively. For the observed number $N_i(< z_i)$ in bin i , the statistical error of $N_i(< z_i)$ is usually considered to be the Poisson error, i.e., $\bar{\sigma}_i = \sqrt{N_i(< z_i)}$, which corresponds to the 68% Poisson confidence intervals for the binned events. Since the observed cumulative number is normalized to $N(0, z_{\max})$ (see Equation 11), the standard deviation errors turn to be $\sigma_i = \sqrt{N_i(< z_i)/N(0, z_{\max})}$. If the accumulated distribution is treated as a sum of independent measurements in the different 40 z bins of width $\Delta z = 0.1$ between $z = 0$ and $z = 4$, the results of fitting the 40 z bins with different M_{\min} are shown in Fig. 3(b) (solid line). We see here that the best fit corresponds to $\log M_{\min} = 8.0^{+0.5}_{-0.5} (1\sigma)^{+0.9}_{-1.2} (2\sigma)$. It is interesting to note that Muñoz & Loeb (2011) found the minimum halo mass capable of hosting galaxies can be around $2.5 \times 10^9 M_{\odot}$ by fitting the observed galaxies luminosity function, in agreement with the minimum halo mass we derive here using GRB data. With $40 - 1 = 39$ degrees of freedom, the reduced χ^2 for the CSFR model with an optimized minimum halo mass is $\chi^2_{\text{dof}} =$

$4.98/39 = 0.13$. Note that taking different values for Δz has very little impact on the best-fit results.

Next, we fix $M_{\min} = 10^{13.0} M_{\odot}$ and keep α as a free parameter. The theoretical GRB cumulative redshift distributions for different values of α are shown in Fig. 4(a). The high halo mass (i.e., $M_{\min} = 10^{13.0} M_{\odot}$) means that the suppression of dark matter halo abundances in this model is very strong, which leads to an unrealistically high value of $\alpha \sim 5.32$ required to be roughly consistent with the observations (blue solid line), with a K-S probability of $P = 0.159$. Using the χ^2 statistic, the constraints on α are shown in Fig. 4(b). For this fit, we obtain $\alpha = 5.32^{+0.17}_{-0.17}(1\sigma)^{+0.34}_{-0.32}(2\sigma)$. With $40 - 1 = 39$ degrees of freedom, the reduced χ^2 is $\chi^2_{\text{dof}} = 39.58/39 = 1.01$. However, such a high value can be ruled out by low- z observations, which imply $\alpha \leq 1.0$ (e.g., Kistler et al., 2009; Robertson & Ellis, 2012; Trenti et al., 2012; Wei et al., 2014). Moreover, Trenti et al. (2012) suggested that there is significant star formation in faint galaxies, it is not possible that the halo mass capable of hosting galaxies can come to be around $10^{13.0} M_{\odot}$.

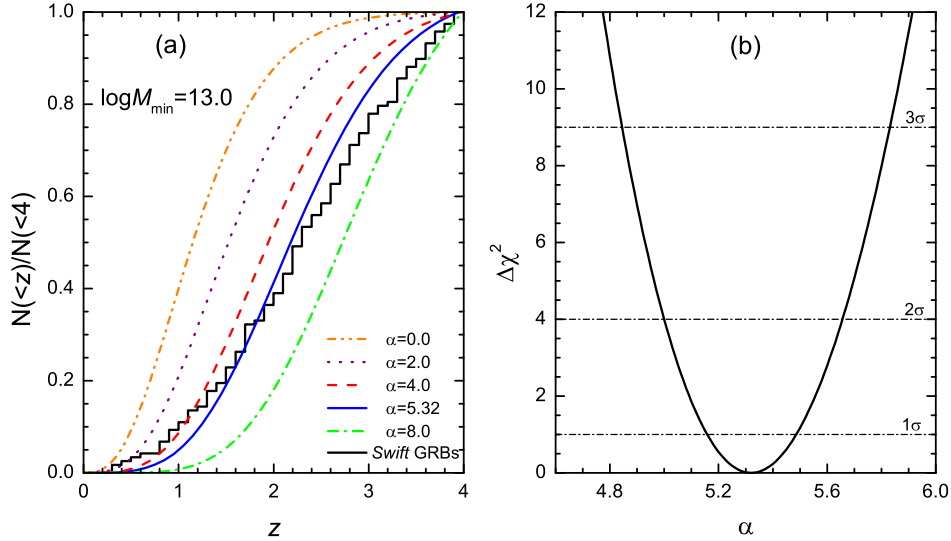


Figure 4: (a): same as Figure 3(a), but the expected redshift distributions are calculated for $M_{\min} = 10^{13.0} M_{\odot}$ while different values of α . From top to bottom, the orange dot-dot-dashed line represents $\alpha = 0.0$, purple dot line $\alpha = 2.0$, red dashed line $\alpha = 4.0$, blue solid line $\alpha = 5.9$, and green dot-dashed line $\alpha = 8.0$. (b): constraints on the evolutionary index, α , for the $M_{\min} = 10^{13.0} M_{\odot}$ model.

| Table 1: Statistical tests of the relevant models | | |
|---|------------------------------------|--------------------------|
| α | $\log M_{\min}$ (M_{\odot}) | K-S test D-stat, Prob |
| 0.0 | 6.0 | 0.0629, 0.7257 |
| 0.0 | 8.0 | 0.0392, 0.9925 |
| 0.0 | 10.0 | 0.1235, 0.0501 |
| 0.0 | 13.0 | 0.5232, 0.0000 |
| 2.0 | 13.0 | 0.3851, 0.0000 |
| 4.0 | 13.0 | 0.1927, 0.0003 |
| 5.32 | 13.0 | 0.1024, 0.1590 |
| 8.0 | 13.0 | 0.2136, 0.0000 |

If we relax the priors, and allow both M_{\min} and α to be free parameters, we can construct confidence limits in the two-dimensional parameter space (M_{\min}, α) by fitting the cumulative redshift distribution of 118 *Swift* GRBs with $z < 4$ and $L_{\text{iso}} > 1.8 \times 10^{51} \text{ erg s}^{-1}$, using the χ^2 statistic. Fig. 5(a) shows the $1\sigma - 3\sigma$ constraint contours of the probability in the (M_{\min}, α) plane. These contours show that at the 1σ level, $-0.54 < \alpha < 0.99$, while M_{\min} is weakly constrained; only an upper limit of $10^{10.5} M_{\odot}$ can be set at this confidence level. The cross indicates the best-fit pair $(\log M_{\min}, \alpha) = (7.2, -0.15)$.

As shown in Fig. 1, the CSFR $\dot{\rho}_{\star}(z)$ is very sensitive to the minimum mass M_{\min} , especially at high- z . To explore the dependence of our results on a possible bias in the high- z bursts, we also consider GRBs with $z < 5$ and $L_{\text{iso}} > L_{\text{lim}}(z = 5) \approx 3.1 \times 10^{51} \text{ erg s}^{-1}$ (consisting of 104 GRBs). These data are delimited by the green shaded region in Fig. 2. Compared to the sub-sample with $z < 4$ and $L_{\text{iso}} > 1.8 \times 10^{51} \text{ erg s}^{-1}$, this new sub-sample has 12 more high- z ($4 < z < 5$) bursts. For the cumulative redshift distribution of these 104 GRBs between $z = 0$ and $z = 5$, the width of z bin $\Delta z = 0.125$ is chosen to ensure the number of z bins (i.e., $n = 40$) is the same as that of the sub-sample with $z < 4$ and $L_{\text{iso}} > 1.8 \times 10^{51} \text{ erg s}^{-1}$. Using the χ^2 statistic, the constraints on the M_{\min} - α plane from these 104 GRBs are shown in Fig. 5(b). It is found that adding 12 high- z GRBs could result in much tighter constraints on M_{\min} . The contours show that models with $\log M_{\min} < 7.7$ and > 11.6 are ruled out at the 1σ confidence level. These are in agreement with what are found by Muñoz & Loeb (2011), in which the minimum halo masses of $\log M_{\min} < 8.5$ and > 9.7 are ruled out at the 95% confidence level.

At the 1σ level, the value of α lies in the range $0.10 < \alpha < 2.55$. The cross indicates the best-fit pair $(\log M_{\min}, \alpha) = (10.5, 1.25)$.

In sum, we find that the redshift distributions of GRBs are consistent with only moderate evolution of $(1+z)^\alpha$ over both $0 < z < 4$ and $0 < z < 5$ ($\sim 1\sigma$ confidence). Compared to previous studies (e.g., Kistler et al., 2009) the results are consistent at the 1σ level, but we obtain a weaker redshift dependence (i.e., weaker enhancement of the GRB rate compared to the CSFR) with lower values of M_{\min} . In addition, the comparison between Fig. 5(a) and Fig. 5(b) may also be summarized as follows: the best-fit results are very different for the two redshift distributions, the distribution of 104 GRBs with $z < 5$ and $L_{\text{iso}} > 3.1 \times 10^{51} \text{ erg s}^{-1}$ (see Fig. 5b) requires a relatively stronger redshift dependence and a higher value of M_{\min} owing to the increased number of high- z GRBs at $4 < z < 5$. Of course, there is also still a lot of uncertainty because of the small high- z GRB sample effect.

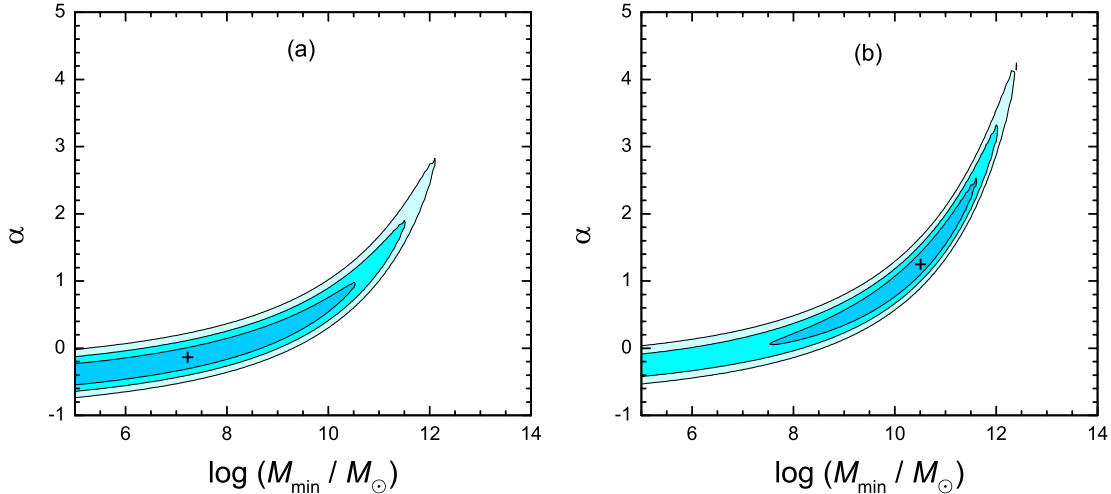


Figure 5: (a): $1\sigma - 3\sigma$ constraint contours for M_{\min} and α , inferred from the cumulative redshift distribution of 118 *Swift* GRBs with $z < 4$ and $L_{\text{iso}} > 1.8 \times 10^{51} \text{ erg s}^{-1}$. The cross indicates the best-fit pair $(\log M_{\min}, \alpha) = (7.2, -0.15)$. (b): same as panel (a), but for 104 *Swift* GRBs with $z < 5$ and $L_{\text{iso}} > 3.1 \times 10^{51} \text{ erg s}^{-1}$. The cross indicates the best-fit pair $(\log M_{\min}, \alpha) = (10.5, 1.25)$.

5. Future constraints

The results of our analyses suggest that the current *Swift* GRB observations can in fact be used to place some constraints on the minimum dark

matter halo mass. We obtain constraints of $7.7 < \log M_{\min} < 11.6$ at the 1σ confidence level. However, these constraints are not strong, and they have uncertainties because of the small GRB sample effect. To increase the significance of the constraints, one needs a larger sample. In order to investigate how much the constraints could be improved with a larger sample, we perform some Monte Carlo simulations based on the future mission, the Sino-French spacebased multiband astronomical variable objects monitor (*SVOM*). The *SVOM* has been designed to optimize the synergy between space and ground instruments, so it is forecast to observe $\sim 70 - 90$ GRBs yr^{-1} (see, e.g., Salvaterra et al., 2008). We simulate a sample of 450 GRBs, each of which is characterized by a set of parameters denoted as (z, L_{iso}) . The sample size represents an optimistic prediction of 5 yr observations of *SVOM* (see, e.g., Salvaterra et al., 2008; de Souza et al., 2013). The soft gamma-ray telescope ECLAIRs onboard the *SVOM* mission will provides fast and accurate GRB triggers to other onboard telescopes, as well as to ground-based follow-up telescopes. Thanks to a low energy threshold of 4 keV, ECLAIRs will be as sensitive as the *Swift*/BAT for the detection of GRBs (Godet et al., 2014). Therefore, we adopt the same bolometric energy flux threshold of *Swift*, $F_{\text{lim}} = 1.2 \times 10^{-8} \text{ erg cm}^{-2} \text{ s}^{-1}$, for *SVOM*. Our detailed simulation procedures are described as follows:

1. The redshift z is generated randomly from the co-moving number density of GRBs at redshift $z + dz$, i.e., $\mathfrak{R}(z) = \frac{\dot{n}_{\text{GRB}}(z) dV_{\text{com}}}{1+z}$. We consider that the GRB rate follows the CSFR, $\dot{n}_{\text{GRB}}(z) \propto \dot{\rho}_{\star}(z)$. For the CSFR $\dot{\rho}_{\star}(z)$, we adopt the empirical fit model (Hopkins & Beacom, 2006; Li, 2008)

$$\log \dot{\rho}_{\star}(z) = a + b \log_{10}(1 + z) , \quad (13)$$

where

$$(a, b) = \begin{cases} (-1.70, 3.30), & z < 0.993 \\ (-0.727, 0.0549), & 0.993 < z < 3.8 \\ (2.35, -4.46), & z > 3.8 \end{cases} . \quad (14)$$

Since $z < 10$ for the current *Swift* sample, the range of z for our analysis is from 0 to 10.

2. The intrinsic luminosity distribution for LGRBs has been well constrained by Wanderman & Piran (2010), which is a simple broken power law function,

$$\Phi(L) = \begin{cases} (L/L_{\star})^x, & L < L_{\star} , \\ (L/L_{\star})^y, & L > L_{\star} , \end{cases} \quad (15)$$

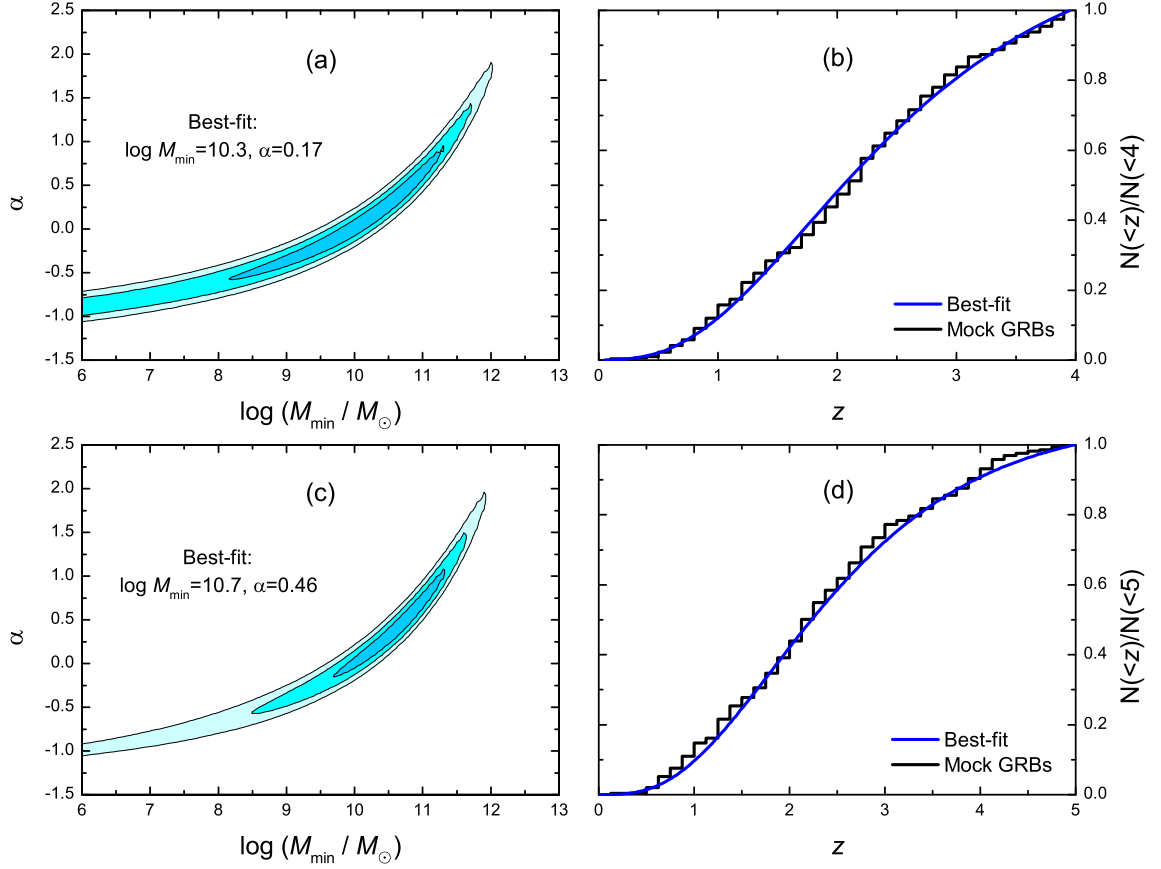


Figure 6: Same as Figure 5, except now for 450 mock GRBs. Left-hand panels: fitted values of M_{\min} and α using the cumulative redshift distribution of 310 mock GRBs with $z < 4$ and $L_{\text{iso}} > 1.8 \times 10^{51} \text{ erg s}^{-1}$ or the distribution of 291 mock GRBs with $z < 5$ and $L_{\text{iso}} > 3.1 \times 10^{51} \text{ erg s}^{-1}$ (right-hand panels; steps). The theoretical curves (right-hand panels; solid lines) correspond to the parameter values that minimize the χ^2 (shown on the left).

where $x = -0.65$, $y = -3$, and $L_\star = 10^{52.05} \text{ erg s}^{-1}$. The mock luminosity L_{iso} is obtained by sampling the probability density function given by Equation (15).

3. With the mock z and L_{iso} , the bolometric energy flux is calculated by $F = L_{\text{iso}}/4\pi D_L^2(z)$. If $F > F_{\text{lim}}$, a mock GRB is recognized as detectable. Otherwise, the mock GRB is excluded.

4. Repeat the above steps to obtain a sample of 450 GRBs.

As described above, we only choose the luminous mock bursts for analysis to reduce the selection effects and also consider two sub-samples (i.e., (S1) the sub-sample with $z < 4$ and $L_{\text{iso}} > 1.8 \times 10^{51} \text{ erg s}^{-1}$ and (S2) the sub-sample with $z < 5$ and $L_{\text{iso}} > 3.1 \times 10^{51} \text{ erg s}^{-1}$) to explore the dependence of our results on a possible bias in the high- z bursts. Using the χ^2 statistic, the constraints on the $M_{\text{min}}-\alpha$ plane from the cumulative redshift distribution of the S1 sub-sample are presented in Fig. 6(a). These contours show that at the 1σ confidence level, we have $8.2 < \log M_{\text{min}} < 11.3$, and $-0.57 < \alpha < 0.95$. The constraints on these two parameters from the S2 sub-sample are also shown in Fig. 6(c). As the results we find in the current *Swift* GRB observations, adding the high- z ($4 < z < 5$) mock GRBs could result in much tighter constraints on M_{min} and relatively higher values of α and M_{min} . The contours show that ~ 5 yr mission of *SVOM* (using the S2 sub-sample) would be sufficient to rule out $\log M_{\text{min}} < 9.7$ and > 11.3 models at the 1σ confidence level. The evolutionary index is constrained to be $-0.11 < \alpha < 1.08$ (1σ). From these results, it is evident that as the sample size increases, the constraints on M_{min} and α become tighter than the current constraints using the *Swift* sample.

6. Discussion and Conclusions

Using the hierarchical structure formation scenario, the CSFR can be built in a self-consistent way. In particular, from the hierarchical scenario we can obtain the baryon accretion rate that governs the size of the reservoir of baryons available for star formation in dark matter halos. It is important to note that the minimum halo mass M_{min} plays an important role in star formation, because first stars can only form in structures that are suitably dense. Star formation will be suppressed when the halo mass is below M_{min} . The connection of LGRBs with the collapse of massive stars has provided a good opportunity for probing star formation in dark matter halos.

In this paper, the numerical value of M_{\min} is constrained using the latest *Swift* GRB data. We conservatively consider that the LGRB rate is proportional to the CSFR and an additional evolution parametrized as $(1+z)^\alpha$. In order to reduce the sample selection effects, we adopt a model-independent approach by selecting only luminous GRBs above a fixed luminosity limit, as Kistler et al. (2008) did in their treatment. This approach has two advantages. Firstly, the reliable statistics of the latest LGRB data allow the use of luminosity cuts to fairly compare GRBs in the full redshift range, eliminating the unknown GRB luminosity function. Secondly, by simply normalizing the cumulative redshift distribution of GRBs to the full redshift range, the constant stands for the GRB efficiency factor can be removed.

For each model (M_{\min}, α) , we can calculate the expected cumulative redshift distribution. The confidence limits in the M_{\min} - α plane can be constructed by fitting the observed cumulative redshift distribution, using the χ^2 statistic. Our results show that at the 1σ confidence level, we obtain $M_{\min} < 10^{10.5} M_\odot$ from 118 *Swift* GRBs with $z < 4$ and $L_{\text{iso}} > 1.8 \times 10^{51} \text{ erg s}^{-1}$. We also find that adding 12 high- z ($4 < z < 5$) GRBs (comprised of 104 GRBs with $z < 5$ and $L_{\text{iso}} > 3.1 \times 10^{51} \text{ erg s}^{-1}$) could result in much tighter constraints on M_{\min} , for which, $10^{7.7} M_\odot < M_{\min} < 10^{11.6} M_\odot$ at the 1σ confidence level. Through Monte Carlo simulations, we find that the constraints on M_{\min} and α can be much improved by enlarging the sample size. The simulations show that the future *SVOM* 5-yr observations would tighten these constraints to $10^{9.7} M_\odot < M_{\min} < 10^{11.3} M_\odot$ at the 1σ confidence level.

Previously, with a minimum halo mass of $10^7 - 10^8 M_\odot$ and a moderate outflow efficiency, Daigne et al. (2006) could reproduce both the fraction of baryons in the structures at the present time and the early chemical enrichment of the intergalactic medium. By analysing the star formation history, Bouché et al. (2010) set a strong constraint on the minimum halo mass: $M_{\min} \simeq 10^{11} M_\odot$. Muñoz & Loeb (2011) also suggested that the halo mass at which star formation is suppressed can be limited by matching the observed galaxy luminosity distribution, in which M_{\min} was constrained to be $10^{8.5} M_\odot < M_{\min} < 10^{9.7} M_\odot$ at the 95% confidence level. In the present paper, we propose that M_{\min} can also be constrained using the redshift distribution of *Swift* GRBs, and we obtain some limits on M_{\min} , namely $10^{7.7} M_\odot < M_{\min} < 10^{11.6} M_\odot$ (1σ), which are consistent with the previous results obtained using both the current baryon fraction and the early chemical enrichment of the intergalactic medium, the star formation history, and the galaxy luminosity function. Although the future *SVOM* 5-yr observations

would tighten these constraints to $10^{9.7}M_{\odot} < M_{\min} < 10^{11.3}M_{\odot}$ (1σ), the lower limit value of M_{\min} is above the upper limit given by Muñoz & Loeb (2011), and well above the values of Daigne et al. (2006).

The strong constraints we derived here indicate that LGRBs are a new promising tool for probing star formation in dark matter halos. Of course, if we know the mechanism responsible for the difference between the LGRB rate and the CSFR, we can constrain the minimum mass very accurately using the LGRB data alone and the utility of LGRBs would be further enhanced. Apart from the obvious approach of increasing the sample size of LGRBs in the future, we predict that the constraints on M_{\min} will also be significantly improved by including different types of observational data, such as the data of star formation history, galaxy luminosity distribution, and GRB redshift distribution.

Acknowledgments

We acknowledge the anonymous referee for his/her important suggestions, which have greatly improved the manuscript. We also thank Z. G. Dai, Y. F. Huang, X. Y. Wang, F. Y. Wang, and W. W. Tan for helpful discussions. This work is partially supported by the National Basic Research Program (“973” Program) of China (Grants 2014CB845800 and 2013CB834900), the National Natural Science Foundation of China (grants Nos. 11073020, 10733010, 11133005, 11322328, and 11433009), the One-Hundred-Talents Program, the Youth Innovation Promotion Association (2011231), and the Strategic Priority Research Program “The Emergence of Cosmological Structures” (Grant No. XDB09000000) of the Chinese Academy of Sciences.

References

- Band D. L., 2006, ApJ, 644, 378
- Blain A. W., Natarajan P., 2000, MNRAS, 312, L35
- Bouché N., et al., 2010, ApJ, 718, 1001
- Butler N. R., Bloom J. S., Poznanski D., 2010, ApJ, 711, 495
- Butler N. R., Kocevski D., Bloom J. S., Curtis J. L., 2007, ApJ, 671, 656
- Campisi M. A., Li L.-X., Jakobsson P., 2010, MNRAS, 407, 1972

- Cao X.-F., Yu Y.-W., Cheng K. S., Zheng X.-P., 2011, MNRAS, 416, 2174
- Chary R., Berger E., Cowie L., 2007, ApJ, 671, 272
- Chornock R., et al., 2010, arXiv, arXiv:1004.2262
- Copi C. J., 1997, ApJ, 487, 704
- Cucchiara A., et al., 2011, ApJ, 736, 7
- Daigne F., Olive K. A., Silk J., Stoehr F., Vangioni E., 2006b, ApJ, 647, 773
- Daigne F., Rossi E. M., Mochkovitch R., 2006a, MNRAS, 372, 1034
- de Souza R. S., Mesinger A., Ferrara A., Haiman Z., Perna R., Yoshida N., 2013, MNRAS, 432, 3218
- Elliott J., Greiner J., Khochfar S., Schady P., Johnson J. L., Rau A., 2012, A&A, 539, A113
- Gehrels N., et al., 2004, ApJ, 611, 1005
- Godet O., et al., 2014, SPIE, 9144, 914424
- Greiner J., et al., 2011, A&A, 526, A30
- Guetta D., Piran T., 2007, JCAP, 7, 003
- Hao J.-M., Yuan Y.-F., 2013, ApJ, 772, 42
- Hinshaw G., et al., 2013, ApJS, 208, 19
- Hjorth J., et al., 2012, ApJ, 756, 187
- Hjorth J., et al., 2003, Natur, 423, 847
- Hopkins A. M., 2007, ApJ, 654, 1175
- Hopkins A. M., 2004, ApJ, 615, 209
- Hopkins A. M., Beacom J. F., 2006, ApJ, 651, 142
- Kistler M. D., Yüksel H., Beacom J. F., Hopkins A. M., Wyithe J. S. B., 2009, ApJ, 705, L104

- Kistler M. D., Yüksel H., Beacom J. F., Stanek K. Z., 2008, *ApJ*, 673, L119
- Kouveliotou C., Meegan C. A., Fishman G. J., Bhat N. P., Briggs M. S., Koshut T. M., Paciesas W. S., Pendleton G. N., 1993, *ApJ*, 413, L101
- Krühler T., et al., 2011, *A&A*, 534, A108
- Lamb D. Q., Reichart D. E., 2000, *ApJ*, 536, 1
- Langer N., Norman C. A., 2006, *ApJ*, 638, L63
- Le T., Dermer C. D., 2007, *ApJ*, 661, 394
- Li L.-X., 2008, *MNRAS*, 388, 1487
- Lu R.-J., Wei J.-J., Qin S.-F., Liang E.-W., 2012, *ApJ*, 745, 168
- Muñoz J. A., Loeb A., 2011, *ApJ*, 729, 99
- Paczynski B., 1998, *ApJ*, 494, L45
- Pereira E. S., Miranda O. D., 2010, *MNRAS*, 401, 1924
- Perley D. A., et al., 2009, *AJ*, 138, 1690
- Perley D. A., Perley R. A., 2013, *ApJ*, 778, 172
- Piran T., 2004, *RvMP*, 76, 1143
- Porciani C., Madau P., 2001, *ApJ*, 548, 522
- Press W. H., Schechter P., 1974, *ApJ*, 187, 425
- Qin S.-F., Liang E.-W., Lu R.-J., Wei J.-Y., Zhang S.-N., 2010, *MNRAS*, 406, 558
- Robertson B. E., Ellis R. S., 2012, *ApJ*, 744, 95
- Sakamoto T., et al., 2011, *ApJS*, 195, 2
- Salpeter E. E., 1955, *ApJ*, 121, 161
- Salvaterra R., Campana S., Chincarini G., Covino S., Tagliaferri G., 2008, *MNRAS*, 385, 189

Salvaterra R., et al., 2012, ApJ, 749, 68

Salvaterra R., Chincarini G., 2007, ApJ, 656, L49

Salvaterra R., Guidorzi C., Campana S., Chincarini G., Tagliaferri G., 2009, MNRAS, 396, 299

Scalo J. M., 1986, FCPH, 11, 1

Schmidt M., 1963, ApJ, 137, 758

Schmidt M., 1959, ApJ, 129, 243

Sheth R. K., Tormen G., 1999, MNRAS, 308, 119

Stanek K. Z., et al., 2003, ApJ, 591, L17

Tan W.-W., Cao X.-F., Yu Y.-W., 2013, ApJ, 772, L8

Tan W.-W., Wang F. Y., 2015, MNRAS, 454, 1785

Totani T., 1997, ApJ, 486, L71

Trenti M., Perna R., Levesque E. M., Shull J. M., Stocke J. T., 2012, ApJ, 749, L38

Virgili F. J., Zhang B., Nagamine K., Choi J.-H., 2011, MNRAS, 417, 3025

Wanderman D., Piran T., 2010, MNRAS, 406, 1944

Wang F. Y., Bromm V., Greif T. H., Stacy A., Dai Z. G., Loeb A., Cheng K. S., 2012, ApJ, 760, 27

Wang F. Y., Dai Z. G., 2011, ApJ, 727, L34

Wang F. Y., 2013, A&A, 556, A90

Wei J.-J., Wu X.-F., Melia F., Wei D.-M., Feng L.-L., 2014, MNRAS, 439, 3329

Wijers R. A. M. J., Bloom J. S., Bagla J. S., Natarajan P., 1998, MNRAS, 294, L13

Woosley S. E., 1993, AAS, 25, 894

Woosley S. E., Bloom J. S., 2006, *ARA&A*, 44, 507

Xu C.-Y., Wei D.-M., 2009, *ChA&A*, 33, 151

Yüksel H., Kistler M. D., Beacom J. F., Hopkins A. M., 2008, *ApJ*, 683, L5

Zhang B., 2007, *ChJAA*, 7, 1

Zhang B., Mészáros P., 2004, *IJMPA*, 19, 2385